INSTITUTE OF PHYSICS PUBLISHING SMART MATERIALS AND STRUCTURES
Smart Mater. Struct. **15** (2006) 1785–1793 doi:10.1088/0964-1726/15/6/033

Shape modeling and validation of stress-biased piezoelectric actuators

K Mossi[1,3], M Mouhli[1], B F Smith[1], P P Mane[1] and R G Bryant[2]

[1] Virginia Commonwealth University, Mechanical Engineering, 601 West Main Street, Box 843015, Richmond, VA 23284, USA
[2] NASA Langley Research Center, 6 West Taylor Street, B1293A, Mail Stop 226, Hampton, VA 23681, USA

E-mail: kmmossi@vcu.edu

Received 29 April 2006, in final form 12 September 2006
Published 16 October 2006
Online at stacks.iop.org/SMS/15/1785

Abstract
Piezoelectric composites with a characteristic initial curvature and accompanying residual stresses are capable of enhanced performance, relative to flat actuators. This paper utilizes Rayleigh–Ritz techniques with revisions regarding the effective in-plane resultant force and the effective bending moment. The Rayleigh–Ritz technique is based on the assumption that the stable geometric configuration developed in the actuator after manufacturing is the configuration that minimizes the total potential energy. This energy is a function of the displacement field which can be approximated by either a four-term model or a 23-term model. In this case, Thunder®, a composite of steel, polyimide adhesive, PZT, and aluminum is constructed with varying geometries so that three-dimensional surface topology maps are measured. Numerically, the four-coefficient model produces results that are not comparable to experimental data. The 23-coefficient model generally shows good agreement with the data for all studied actuators. In the case of actuators with a length to width ratio of one, simulations are close to experimental results. In the case of length to width ratios different to unity, the model accurately predicts the devices' shape. It is further demonstrated that the curvature of the devices seems to follow the rolling direction of the stainless steel layer, challenging the isotropy assumption.

(Some figures in this article are in colour only in the electronic version)

1. Introduction

From 1980 to the present, research on material development for the design of high performance aerospace industrial and biomedical applications, based on ferroelectric and piezoelectric materials, has burgeoned (Smith 2005). Beams, trusses structures, plate and shell-like structures are frequently used as host structures for piezoelectric sensors and actuators for vibration and noise control applications. Several designs have been conceived experimentally such as vibration control for plates (Bayer *et al* 1991), for beams (Bailey and Hubbard 1985), and buckling control (Thomson and Loughlan 1995).

The type of materials utilized in these host structures are piezoelectric transducers that can generate large displacements (Newnham and Ruschau 1991) while the transducer is subjected to a sizable load. This characteristic is deemed essential for actuator applications (Uchino 2000).

A number of transducer designs based on piezoelectric ceramics have been developed to address this issue, in particular stress-biased actuators. Thunder®, a type of pre-stressed laminate, has been the subject of intense investigation (Capozzoli *et al* 1999, Granger *et al* 2000, Ballato 2001, Lee *et al* 2002, Aimmanee and Hyer 2004, Lee *et al* 2004, Usher and Sim 2005, Yoon *et al* 2005) due to its unique performance characteristics compared to a Unimorph® and a Bimorph device, as well as traditional direct extensional

[3] Author to whom any correspondence should be addressed.

actuators. These stress-biased devices are composite structures that incorporate a piezoelectric layer bonded to a metal, glass/epoxy or cermet layer. While the specifics of the fabrication procedures differ for those actuators, for all, a domed structure, with varying degrees of curvature, is formed after processing.

There have been a number of studies (Benjeddou *et al* 1997) that have attempted to investigate the factors that contribute to the improved performance of these devices. Device aspects such as mass loading, engineering mechanics, hysteresis (Smith *et al* 2003) and enhanced domain switching, due to the presence of tensile stresses within the upper portion of the piezoelectric layer, have all been reported to contribute to the increased displacement response that is observed. While further work is required to better understand the relative importance of these different factors, a number of investigations (Wieman *et al* 2001) have been carried out that have begun to provide insight in this area. These studies have employed a range of techniques, including finite-element analysis (Goo *et al* 2005, Taleghani and Campbell 1999), equivalent circuit modeling (Nothwang *et al* 2000) and the use of Unimorph theory to predict device shape and electromechanical response (Ballato *et al* 2001).

Wang *et al* (2002) and Wang and Cross (1999) developed equations that identify the impact of variables such as device geometry on a pre-stressed Rainbow actuator. The results of this work imply that mechanical aspects alone cannot satisfactorily explain observed performance of the devices.

A modified approach based on Unimorph theory was later used by Schwartz to quantify the mechanics contributions to Rainbow performance (Schwartz *et al* 2001). Depending upon device fabrication conditions, the mechanics contribution to overall performance was observed to vary from a high of 72% to a low of 53%, for an applied electric field of 10 kV cm^{-1}.

Various modeling methods and control schemes have already been proposed to enhance the controllability of piezoelectric actuators (Takahashi 1986). For example, Crawley and de Luis (1987) and Crawley and Anderson (1990), have proposed an analytical model for segmented piezoelectric actuators. The model consists of a Bernoulli–Euler beam with piezoelectric actuators bonded to a surface or embedded in a laminate.

Numerical models (Saravanos 1997) using finite-element analysis (Hwang and Park 1993) have been used to predict the actuator shape, such as the work done by Soderkvist (1996) for the beam case, Smith (2005) for the plate model, and Kennedy *et al* (2001) for different Thunder® actuators. The latter compared dome height of the actuators with accuracy between 0.5% and 40.8%.

Another approach utilizes the Rayleigh–Ritz techniques (Young 1950), which minimizes the total potential energy assuming that the stable configuration developed in the actuator due to cooling is the configuration that minimizes the total potential energy of the actuator. This type of analysis has been used to predict the shape of cooled actuators such as Thunder® as demonstrated by Aimmanee and Hyer (2004), (2006), and Zhang and Sun (1999). Aimmanee and Hyer (2004, 2006) in particular have modeled the shape of Rainbow, Thunder®, and Lipca specialty actuators comparing the results to those obtained with a finite-element simulation. Revisions made to their work regarding the effective in-plane resultant force, and the effective bending moment, are the main focus of this work as well as validating the results with experimental data. The Rayleigh–Ritz technique and classical lamination theory with the inclusion of geometric nonlinearities are used to predict the room-temperature shapes of the Thunder® actuator. Code is written using the programming software Mathematica and built upon the work done by Dano and Hyer (1998).

2. Classical laminate theory

Classical lamination theory is an expansion of Kirchhoff linear theory for homogeneous plates to laminated plates. Hyer (1981, 1982) showed that classical lamination theory cannot always accurately predict the room-temperature shapes of asymmetric laminates (Lee 1990); however, if geometric nonlinearities are included in the theory, by using nonlinear strain–displacement equations, the shape could be predicted more accurately. In classical lamination theory (Banks *et al* 1996), a number of simplifying assumptions are made, including: (1) the actuator thickness is very small in comparison with the other dimensions such as radius or length. This condition is important to thin plate theory, which states that the ratio of the actuator thickness to the smallest radius of curvature is small as compared to unity. For all Thunder® actuators used in this study, this condition was satisfied. (2) The actuator deformations are sufficiently small (the deflection is much less than the thickness). Since piezoelectric actuators often vibrate at large amplitudes, the linear theory is not adequate; therefore this hypothesis is relaxed and nonlinear Von Karman terms are included in the strain formulation. (3) The stress in the direction normal to the thin dimension are taken to be negligible. This assumption, in combination with the fourth, deals with the constitutive properties of thin shells and allows the three-dimensional elasticity problem to be reduced into a two-dimensional one. (4) A line which is originally normal to the shell reference surface will remain normal to the deformed reference surface and will remain unstrained. (5) The interfaces between adjacent layers are perfectly bonded. (6) The stable dome-like configuration developed in the actuator due to the mismatch of coefficients of thermal expansion is the configuration that minimizes the potential energy of the actuator. (7) Isotropic material behavior for each layer. (8) Tabs or extension though included in the construction of the actuator by making the backbone (bottom) layer longer than the other layers are not included in the calculations.

A cartesian coordinate system is used for the analysis and the origin of the coordinate system is chosen at the geometric center of the actuator as shown in figure 1.

The total potential energy of the actuator, the stress strain relations for each layer are utilized as described by the work of Hyer and Jilani (1998). Potential energy, Π, is given by

$$\Pi = \tfrac{1}{2} \iiint \Big[\left(\sigma_x - \sigma_x^{\mathrm{T}}\right) \cdot \varepsilon_x + \left(\sigma_y - \sigma_y^{\mathrm{T}}\right) \cdot \varepsilon_y + \tau_{xy} \cdot \gamma_{xy} \Big] \cdot \mathrm{d}x \cdot \mathrm{d}y \cdot \mathrm{d}z \qquad (1)$$

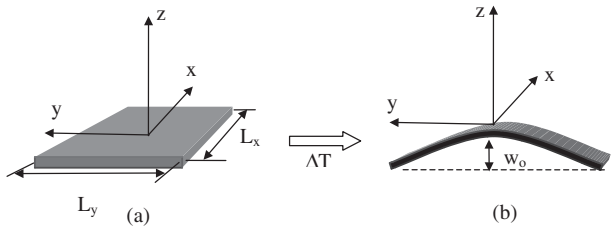

Figure 1. (a) Initial and (b) cooled shapes of an actuator and coordinate system.

where the integral is over the volume of the actuator, σ represents the stress in the x, y and z directions, σ^{T} represents the thermally induced stresses, and ε and γ_{xy} are the normal and shear strains in the actuator. Assuming isotropic material behavior for each layer, the stress–strain relations for a given layer are defined by

$$\begin{aligned}\sigma_x &= Q\cdot(\varepsilon_x-\alpha\cdot\Delta T)+\nu\cdot Q\cdot\left(\varepsilon_y-\alpha\cdot\Delta T\right)\\ \sigma_y &= \nu\cdot Q\cdot(\varepsilon_x-\alpha\cdot\Delta T)+Q\cdot\left(\varepsilon_y-\alpha\cdot\Delta T\right)\\ \tau_{xy} &= \tfrac{1}{2}\cdot(1-\nu)\cdot Q\cdot\gamma_{xy}\end{aligned}\tag{2}$$

and

$$\begin{aligned}Q &= \frac{Y}{1-\nu^2}\\ \sigma^{\mathrm{T}} &= \sigma_x^{\mathrm{T}}=\sigma_y^{\mathrm{T}}=(1+\nu)\cdot Q\cdot\alpha\cdot\Delta T\end{aligned}\tag{3}$$

where Y is the Young's modulus of the material, and ν and α are the Poisson ratio and the coefficient of thermal expansion, respectively, and the thermal stresses, σ^{T}, in the x and y directions are the same. The temperature change due to cooling is ΔT and is assumed to be spatially uniform. The material properties are assumed to be temperature independent. So that combining equation (3), the thermal stresses become

$$\begin{aligned}\sigma^{\mathrm{T}} &= (1+\nu)\cdot\frac{Y}{1-\nu^2}\cdot\alpha\cdot\Delta T\\ &= \cancel{(1+\nu)}\cdot\frac{Y}{(1-\nu)\cdot\cancel{(1+\nu)}}\cdot\alpha\cdot\Delta T\\ \sigma^{\mathrm{T}} &= \frac{Y}{1-\nu}\cdot\alpha\cdot\Delta T.\end{aligned}\tag{4}$$

Integrating equation (1) with respect to z the total potential energy gives

$$\begin{aligned}\Pi = \tfrac{1}{2}\int_{-\frac{L_x}{2}}^{+\frac{L_x}{2}}\cdot\int_{-\frac{L_y}{2}}^{+\frac{L_y}{2}}\Big[&\left(N_x-N^{\mathrm{T}}\cdot\Delta T\right)\cdot\varepsilon_x^0\\ &+\left(N_y-N^{\mathrm{T}}\cdot\Delta T\right)\cdot\varepsilon_y^0+N_{xy}\cdot\gamma_{xy}^0\\ &+\left(M_x-M^{\mathrm{T}}\cdot\Delta T\right)\cdot\kappa_x^0\\ &+\left(M_y-M^{\mathrm{T}}\cdot\Delta T\right)\cdot\kappa_y^0+M_{xy}\cdot\kappa_{xy}^0\Big]\cdot\mathrm{d}x\cdot\mathrm{d}y\end{aligned}\tag{5}$$

where N_s and M_s are respectively the force and the moment resultants within the actuator and are given in detail in Aimmanee and Hyer (2004). In particular, N^{T} and M^{T} are material properties that involve, additionally, the coefficients of thermal expansion of each layer and are given by

$$\begin{aligned}N^{\mathrm{T}} &= \sum_{k=1}^{n}\frac{E_k\cdot\alpha_k\cdot(z_k-z_{k-1})}{1-\nu_k}\\ M^{\mathrm{T}} &= \frac{1}{2}\sum_{k=1}^{n}\frac{E_k\cdot\alpha_k\cdot(z_k^2-z_{k-1}^2)}{1-\nu_k}.\end{aligned}\tag{6}$$

Since N^{T} and M^{T} are functions of the thermal stresses integrated through the thickness, their functional forms differ from those found in Aimmanee and Hyer (2004). In Aimmanee and Hyer's work, the denominator of the expression for thermal stress is $1-\nu_k^2$, whereas in the present study a revision has been made to this term as outlined by equation (4), leaving the denominator as $1-\nu_k$.

The strain field is given by the Kirchhoff hypothesis as

$$\begin{aligned}\varepsilon_x &= \varepsilon_x^0+z\cdot\kappa_x^0\\ \varepsilon_y &= \varepsilon_y^0+z\cdot\kappa_y^0\\ \gamma_{xy} &= \gamma_{xy}^0+z\cdot\kappa_{xy}^0\end{aligned}\tag{7}$$

where the reference surface strain including the non linear Von-Karman terms are defined by

$$\begin{aligned}\varepsilon_x^0 &= \frac{\partial u_0}{\partial x}+\frac{1}{2}\cdot\left(\frac{\partial w_0}{\partial x}\right)^2\\ \varepsilon_y^0 &= \frac{\partial v_0}{\partial y}+\frac{1}{2}\cdot\left(\frac{\partial w_0}{\partial y}\right)^2\\ \gamma_{xy}^0 &= \frac{\partial u_0}{\partial y}+\frac{\partial v_0}{\partial x}+\frac{1}{2}\cdot\left(\frac{\partial w_0}{\partial x}\right)\cdot\left(\frac{\partial w_0}{\partial y}\right).\end{aligned}\tag{8}$$

The values for u_o, v_o, and w_o in equations (7) and (8) are the three components of displacement of a point on the reference surface in the x, y and z directions, respectively, given by the Rayleigh–Ritz approximations. The reference surface curvatures are given by

$$\begin{aligned}\kappa_x^0 &= -\frac{\partial^2 w_0}{\partial x^2}\\ \kappa_y^0 &= -\frac{\partial^2 w_0}{\partial y^2}\\ \kappa_{xy}^0 &= -2\cdot\frac{\partial^2 w_0}{\partial x\cdot\partial y}.\end{aligned}\tag{9}$$

For the four-coefficient model, equation (10) is utilized (Hyer and Jilani 1998).

$$\begin{aligned}w^0(x,y) &= \tfrac{1}{2}(a\cdot x^2+b\cdot y^2)\\ u^0(x,y) &= c\cdot x-\frac{a^2\cdot x^3}{6}-\frac{a\cdot b\cdot x\cdot y^2}{4}\\ v^0(x,y) &= d\cdot y-\frac{b^2\cdot y^3}{6}-\frac{a\cdot b\cdot x^2\cdot y}{4}.\end{aligned}\tag{10}$$

Table 1. Mechanical properties of the layers used in a Thunder® device.

Material	Modulus of elasticity Y (N m^{-2})	Poisson's ratio ν	CTE α (μm m^{-1} °C^{-1})	Strain/field piezoelectric constant d_{31} (m V^{-1})
Aluminum[a]	7.00×10^{10}	0.33	24	—
SI	3.45×10^{9}	0.40	45	—
PZT[b]	6.70×10^{10}	0.31	3.0	-1.7×10^{-10}
Stainless steel[c]	1.93×10^{11}	0.25	17	—

[a] ASTM B209.
[b] PZT-5A CTS wireless.
[c] Stainless steel type 302, ASTM A666, full hard.

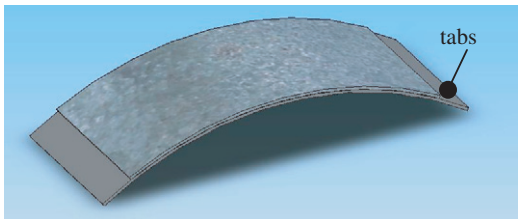

Figure 2. Thunder® piezoelectric actuator.

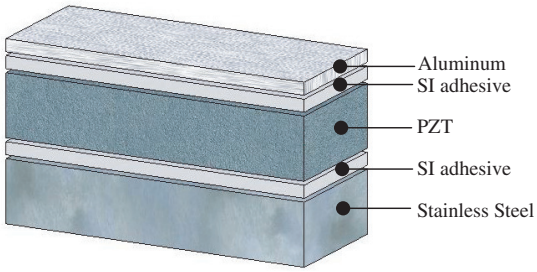

Figure 3. Thunder® constituent layers.

For the 23-coefficient model, equation (11) is used.

$$\begin{aligned} w_0(x,y) &= c_1 \cdot x^2 + c_2 \cdot y^2 + c_3 \cdot x^4 + c_4 \cdot y^4 + c_5 \cdot x^2 \cdot y^2 \\ &\quad + c_6 \cdot x^4 \cdot y^2 + c_7 \cdot x^2 \cdot y^4 + c_8 \cdot x^6 + c_9 \cdot y^6 \\ u_0(x,y) &= c_{10} \cdot x + c_{12} \cdot x^3 + c_{14} \cdot x \cdot y^2 + c_{16} \cdot x^5 \\ &\quad + c_{18} \cdot x^3 \cdot y^2 + c_{20} \cdot x \cdot y^4 + c_{22} \cdot x^7 \\ v_0(x,y) &= c_{11} \cdot y + c_{13} \cdot y^3 + c_{15} \cdot x^2 \cdot y + c_{17} \cdot y^5 \\ &\quad + c_{19} \cdot x^2 \cdot y^3 + c_{21} \cdot y \cdot x^4 + c_{23} \cdot y^7. \end{aligned} \tag{11}$$

Coefficients a, b, c, and d from equation (10) and coefficients c_1 through c_{23} from equation (11) are unknown but are to be determined by minimizing the total potential energy as demonstrated by Aimmanee and Hyer.

3. Thunder® actuator manufacturing and characterization

Thunder® (Face International Corporation) shown in figure 2, is a composite laminate consisting of a metal substrate, SI adhesive, (Imitec Incorporated) lead zirconate titanate (PZT), and a top metal layer that is formed when the composite laminate is heated under pressure to temperatures that allow the adhesive top bond and then cooled to room temperature. The construction of Thunder® actuators requires an oven equipped with a vacuum fixture and an operating temperature of 350 °C, an air brush, and an autoclave with a minimum capability of 207 kPa and 350 °C. The procedure for the manufacturing of Thunder® is presented in detail elsewhere (Mossi *et al* 1998).

During the cooling phase (Mossi *et al* 1998), the adhesive, at a highly viscous state at the bonding temperature, solidifies. Consequently, internal stresses are developed in the constituent materials due to the differing coefficient of thermal expansion between the layers. This process produces the characteristic curved shape resulting from pre-stress.

Table 2. Actuator constituent layers thickness in mm prior to manufacturing.

Type	PZT	Steel	Adhesive	Aluminum
6R	0.3810	0.2540	0.0254	0.0254
7R	0.2540	0.2032	0.0254	0.0254
7RX	0.2540	0.2032	0.0254	0.0254
8R	0.2032	0.1524	0.0254	0.0254
9R	0.2032	0.1524	0.0254	0.0254
10R	0.2032	0.1524	0.0254	0.0254

Additionally, the backing metal layer provides robustness that allows the generation of relatively large distributed strains without damaging the actuator (Navapan-Traiphol *et al* 2004, Bryant *et al* 2005). The combination of robustness and curvature or pre-stress enhancement provides Thunder® with high displacement capabilities (Mulling *et al* 2001, Schwartz and Narayanan 2002) such that a potential for applications including high speed valve design, synthetic jets for flow control and linear motor component for micro robotics (Palmer *et al* 2004) are now feasible.

For the specific Thunder® actuators studied here, five rectangular layers are considered as shown in figure 3.

The material properties for each metal layer and for the ceramic layer, a soft-PZT, and a polyimide layer, SI, are shown in table 1.

The different dimensions of the layers for the Thunder® actuators prior to manufacturing as well as the overall dimensions after manufacturing are described in tables 2 and 3 respectively.

After manufacturing, in addition to the overall physical dimensions, the surface topology of each device is measured using a Fanamation 606040 coordinate axis machine to 8.1 μm

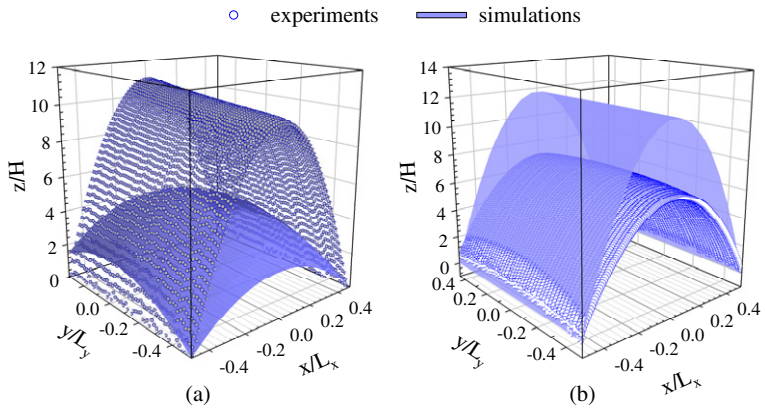

Figure 4. Rayleigh–Ritz four-coefficient model predicted curvature versus experimental data for Thunder® models with a ratio (a) $L_y/L_x \cong 1$ (model 7R) and (b) $L_y/L_x \geqslant 1$ (model 7RX).

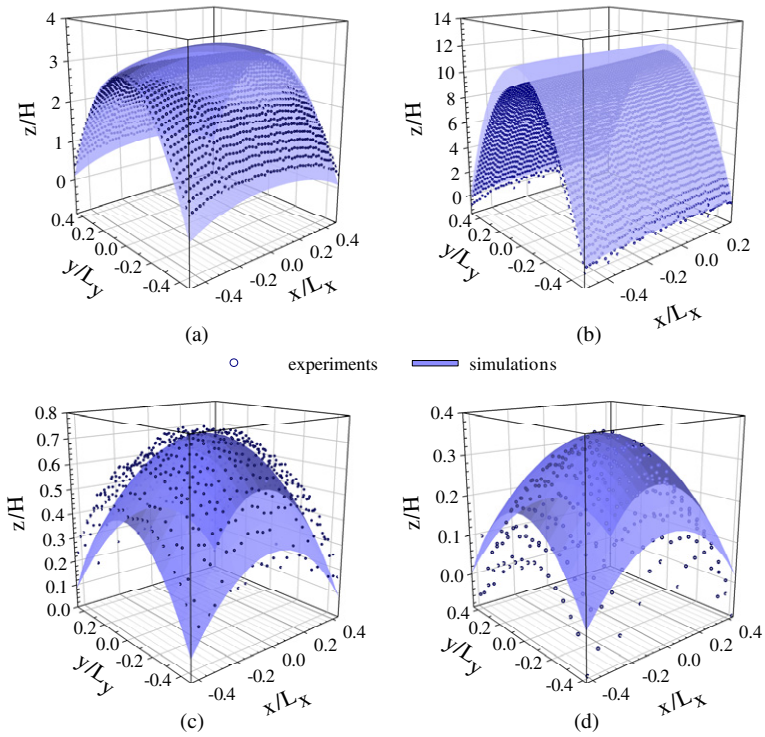

Figure 5. Rayleigh–Ritz 23-coefficient model predictions of curvature versus experimental data for Thunder® models with $L_y/L_x \cong 1$, models (a) 7R; (b) 6R; (c) 10R; and (d) 9R.

accuracy. The surfaces of the devices are prepared by lightly sanding the top surface with 400 grit emery paper and are cleaned with isopropanol.

4. Results

During manufacturing, stresses develop during the cooling phase and the devices remain flat until the pressure is released after they are cooled. The model used in this study, as developed by Hyer, does not incorporate this force but rather assumes the actuator is free to deform as the curing temperature is diminished. Alternatively, if the cured actuator was heated from the room-temperature condition, the shape as a function of elevated temperature could also be predicted.

Modeling results are obtained using the specific material properties given in table 1 assuming that bonding temperature, T_c, of the adhesive for Thunder® occurs at 325 °C and room temperature is 25 °C. Thus for a Thunder® actuator, the temperature at the beginning of the cooling process is T_c of 325 °C; and the end of the cooling process, the temperature is 25 °C, which corresponds to $\Delta T = -300$ °C. The adhesive, SI layer, has a transition temperature of 260 °C, however

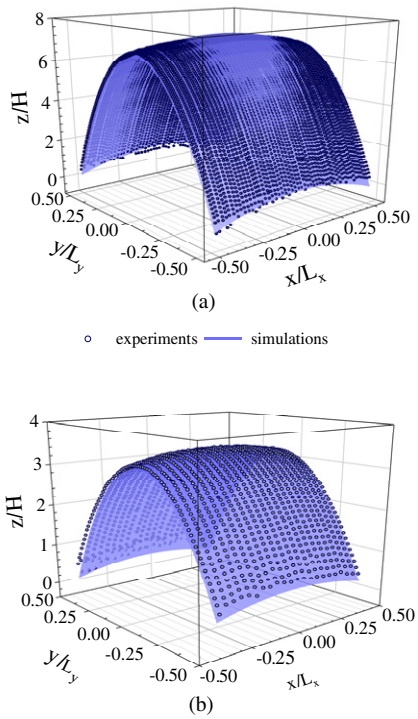

Figure 6. Rayleigh–Ritz 23-coefficient model prediction of curvature versus experimental data for Thunder® models with a ratio $L_x/L_y \neq 1$ (a) 7RX and (b) 7R.

to ensure the polyimide layer melts, the composite is taken approximately 50 °C above its transition temperature.

4.1. Four-coefficient model

The results of the four-term model of a Thunder® type actuator do not closely represent the shape of any of the actuators used in this study, as predicted by Aimmanee where predictions are compared to finite-element analysis (Aimmanee and Hyer 2004). In this case, the results are compared with experimental data as shown in figures 4(a) and (b). These figures show typical results for two devices that have a different aspect ratio, $L_y/L_x = 1.05$ and $L_y/L_x = 2.8$, respectively. In the case of $L_y/L_x \cong 1.0$, figure 4(a), the model under-predicts the curvature of the device by more than 30% at its highest point (dome height). In the case of $L_y/L_x \cong 3$, figure 4(b), the model over-predicts the curvature by 40%. As a result, it is seen that the shape predicted by the four-term model is not in agreement with the shape of a real actuator and the multiple coefficient model may be more appropriate.

4.2. Multiple-coefficient model

Since the minimization process involves taking the first derivative of the total potential energy, equation (1), and equating it to zero, a maximum of the total potential energy, an unstable mode, may be found instead. Stability is studied by taking the second derivative with respect to the unknown coefficients, which leads to a 23 by 23 symmetric matrix of second derivatives of the total potential energy. This stability of the predicted shapes is insured if the matrix is positive definite.

Table 3. Actuators dimensions after manufacturing.

Type	Dimensions[a] (mm) length × width	L_y/L_x	Total thickness (±0.025 mm)	PZT thickness (mm)
6R	51.816 × 50.419	1.03	0.711	0.381
7R	73.406 × 69.850	1.05	0.533	0.254
7RX	69.850 × 24.892	2.81	0.533	0.254
8R	37.846 × 13.716	2.76	0.432	0.203
9R	10.541 × 09.398	1.12	0.432	0.203
10R	13.716 × 12.624	1.09	0.432	0.203

[a] Overall length and width excluding tabs.

Table 4. Actuators dimensions after manufacturing.

Type	Dimensions[a] (mm) length × width	L_y/L_x	Total thickness (±0.025 mm)	PZT thickness (mm)
4JR	29.46 × 29.46	1	0.526	0.203
5JR	55.09 × 29.39	1.87	1.562	0.414

[a] Devices constructed without tabs.

The shapes at room temperature as predicted by the multi (23) coefficients model are illustrated in figures 5(a)–(d) for devices where $L_y/L_x \cong 1.0$. These shapes are a close match to the experimental data, however small discrepancies can be observed in the overall shape.

Figures 6(a) and (b) show results for devices where $L_y/L_x \neq 1.0$, where numerical and experimental results closely match.

These discrepancies between experimental and numerical work may be explained by the variations in the materials properties of the constituent layers of the device, specifically the stainless steel layer. The type of metal used is a rolled full hard stainless steel. One of the assumptions made for the technique utilized in this work is that the materials utilized are isotropic. In the case of the stainless steel layer, this assumption may not hold true. Some evidence of the grain-orientation of cold-rolled stainless steel has been shown by Wang *et al* (2002). In their work, they showed strong grain orientation anisotropy in a cold-rolled sample.

To offer some evidence of the hypothesis of the anisotropy of the stainless steel layer, devices with the roll direction clearly identified were constructed and tabs were eliminated to avoid any influence the tabs have on the devices final shape. These devices were manufactured such that the main difference on the manufactured devices, 4JR and 5JR, in this case is the length to width ratio, L_y/L_x, as shown in table 4 where the number of layers and the material types of each layer were kept the same as the rest of the samples utilized here.

Simulations and experiments in this case are similar to the other manufactured samples as shown in figure 7(a) for 4JR, a square sample, and figure 7(b) for 5JR, a rectangular sample. In the case of an aspect ratio, $L_y/L_x \cong 1$, experimental and numerical predictions differ; in the case of $L_y/L_x > 1$, experimental and numerical results are in agreement, assuming that L_y is taken as the long axis. In the case of figure 7(b) for a 5JR sample, the length dominates the shape of the device, minimizing anisotropy effects. In the case of figure 7(a), the directionality of the stainless steel becomes evident.

To illustrate the effect of length on the final shape of the device, and perhaps the anisotropy of the stainless steel layer,

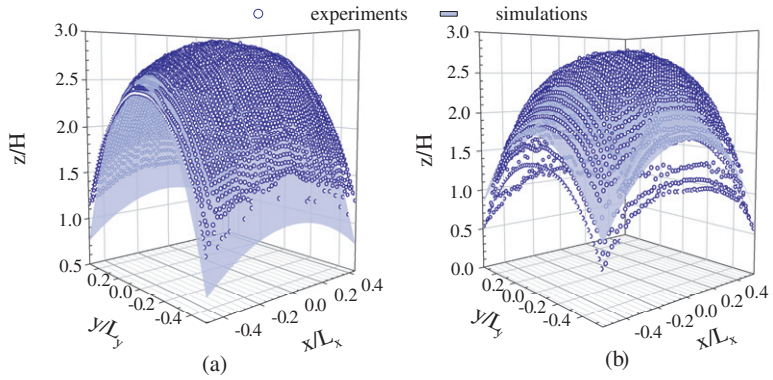

Figure 7. Rayleigh–Ritz 23-coefficient prediction of curvature versus experimental with a 23-coefficient model for a Thunder® device with (a) $L_y = L_x$ (model J4R) and (b) $L_y \neq L_x$ (model J5R).

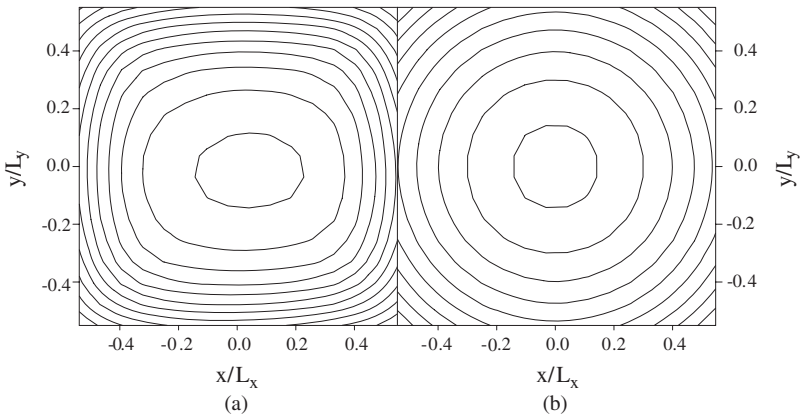

Figure 8. Contour plots for (a) experimental and (b) predicted.

Table 5. Geometrical factors for all actuators.

Type	L_y/L_x	L_y/t
6R	1.03	73
7R	1.05	138
7RX	2.81	131
8R	2.76	88
9R	1.12	24
10R	1.09	32
4JR	1.00	56
5JR	1.87	35

contour plots of the two samples are shown in figures 8(a) and (b) for experimental and numerical results respectively. In the case of the experimental results for the square sample, figure 8(a), the larger curvature follows the rolling direction of the stainless steel, x-direction. This figure shows an oval contour shape versus simulations, figure 8(b) a circular shape.

Further analysis performed by Aimmanee and Hyer on the shape stability of these devices is considered as another possible reason for the discrepancies. The stability criterion was calculated, table 5, and compared to the results shown by Aimmanee and Hyer, to test the possibility of manufacturing a sample close to a point where more than one solution to the curvature is possible. The results showed that no piece was close to the bifurcation or instability point.

The results however show that the Rayleigh–Ritz technique with 23 coefficients is an effective tool in predicting the shape of these actuators as long as the sidelength/width ratio, $L_y/L_x \neq 1$, is different to 1. Further refinement of the model for $L_y/L_x = 1$ may be needed so that the incorporation of the stainless anisotropy may be realized.

5. Conclusions

Experimental verification of the work presented by Aimmanee and Hyer on the four-coefficient model and the 23-coefficient model using Rayleigh–Ritz techniques is presented. Three-dimensional topographical maps of an array of devices of varying geometries are performed and compared to the simulations performed. Results for the four-coefficient model appear to differ significantly from the experimental data even in the cases where the devices' ratio is square. The work by Aimmanee and Hyer states that when $L_y = L_x$, the four-term model is fairly accurate when compared to finite-element analysis results. In this study, the four-term model under-predicts the curvature and overall shape for $L_y = L_x$, and over-predicts it for the $L_y/L_x \neq 1$. In the case of the 23-coefficient model, the overall shape is predicted accurately for all the samples tested. In some cases, namely $L_y = L_x$, there were discrepancies on the predicted shape and in cases where $L_y/L_x \neq 1$ the results matched accurately. This phenomenon

may be due to the assumption of the model that the layers on the composite are isotropic. To test this assumption, devices with the roll-direction of the bottom layer of the composite identified were constructed, one with $L_y = L_x$ and one with $L_y \neq L_x$. Experimental results showed that the devices tend to have directionality and follow the rolling direction of the stainless steel and hence the isotropy assumption does not hold. In the samples where $L_y \neq L_x$, the model predicts the device shape accurately perhaps because the anisotropy of the stainless steel layer effect is minimized by the dominant dimension. Further modification of the model as well as further characterization of the individual materials used in the construction of these devices may be necessary for the optimal design of these actuators.

Acknowledgments

This work is supported under NASA Grant NNL04AA04G and the work of Mr Jon Robbins at the Smart Materials Lab.

References

Aimmanee S and Hyer M W 2004 Analysis of the manufactured shape of rectangular THUNDER-type actuators *Smart Mater. Struct.* **13** 1389–406

Aimmanee S and Hyer M W 2006 A comparison of the deformations of various piezoceramic actuators *J. Intell. Mater. Syst. Struct.* **17** 167–86

Bailey T and Hubbard J E 1985 Distributed piezoelectric-polymer active vibration control of a cantilever beam *J. Guid. Control Dyn.* **8** 605–11

Ballato A 2001 Modeling piezoelectric and piezomagnetic devices and structures via equivalent networks *IEEE Trans. Ultrason. Ferroelectr. Freq. Control* **48** 1189–240

Ballato J, Schwartz R and Ballato A 2001 Network formalism for modeling functionally gradient piezoelectric plates and stacks and simulations of RAINBOW ceramic actuators *IEEE Trans. Ultrason. Ferroelectr. Freq. Control* **48** 462–76

Banks H T, Smith R C and Wang Y 1996 *Smart Material Structures Modeling, Estimation and Control* (Chichester: Wiley)

Bayer J I, Varadan V V and Varadan V K 1991 Discrete piezoelectric sensors and actuators for active control of two-dimensional spacecraft components *Proc. Int. Soc. Opt. Eng.* **1480** 102–14

Benjeddou A, Trindade M A and Ohayon R 1997 A unified beam finite element model for extension and shear piezoelectric actuation mechanisms *J. Intell. Mater. Syst. Struct.* **8** 1012–25

Bryant R G, Mossi K M, Robbins J A and Bathel B F 2005 The correlation of electrical properties of prestressed unimorphs as a function of mechanical strain and displacement *Integr. Ferroelectr.* **71** 267–87

Capozzoli M, Gopalakrishnan J, Hogan K, Massa J, Tokarchik T, Wilmarth S, Banks H T, Mossi K M and Smith R C 1999 Modeling aspects concerning THUNDER® actuators *Proc. Int. Soc. Opt. Eng.* **3667** 719–27

Crawley E F and Anderson E 1990 Detailed models of piezoceramic actuation of beams *J. Intell. Mater. Syst. Struct.* **1** 4–25

Crawley E F and de Luis J 1987 Use of piezoelectric actuators as elements of intelligent structures *AIAA J.* **25** 1373–85

Dano M L and Hyer M W 1998 Thermally-induced deformation behavior of unsymmetric laminates *Int. J. Solids Struct.* **35** 2102–20

Goo N S, Haris A, Park H C and Yoon K J 2005 Validation of a laminated beam model of Lipca piezoelectric actuators *J. Intell. Mater. Syst. Struct.* **16** 189–95

Granger R, Washington G and Kwak S K 2000 Modeling and control of a singly curved active aperture antenna using curved piezoceramic actuators *J. Intell. Mater. Syst. Struct.* **11** 225–33

Hwang W S and Park H C 1993 Finite element modeling of piezoelectric sensors and actuators *AIAA J.* **31** 930–7

Hyer M W 1981 Calculations of the room-temperature shapes of unsymmetric laminates *J. Compos. Mater.* **15** 296–309

Hyer M W 1982 The room-temperature shapes of four-layer unsymmetric cross-ply laminates *J. Compos. Mater.* **16** 318–28

Hyer M W and Jilani A 1998 Predicting the deformation characteristics of rectangular unsymmetrically laminated piezoelectric materials *Smart Mater. Struct.* **7** 784–91

Kennedy C, Ucher T, Mulling J and Kingon A 2001 Modeling and simulation of Thunder actuators using ANSYS finite-element analysis *Modeling Simul. Microsyst.* 330–3

Lee C K 1990 Theory of laminated piezoelectric plates for the design of distributed sensors/actuators. Part I: Governing equations and reciprocal relationships *J. Acoust. Soc. Am.* **87** 1144–58

Lee S, Cho B C, Park H C, Yoon K J and Goo N S 2002 Analysis of multi-layered actuators using an assumed strain solid element *Mater. Chem. Phys.* **75** 174–7

Lee S, Cho B C, Park H C, Goo N S and Yoon K J 2004 Piezoelectric actuator-sensor analysis using a three-dimensional assumed strain solid element *J. Intell. Mater. Syst. Struct.* **15** 329–38

Mossi K M, Selby G V and Bryant R G 1998 Thin-layer composite unimorph ferroelectric driver and sensor properties *Mater. Lett.* **35** 39–49

Mulling J, Usher T, Dessent B, Palmer J, Franzon P, Grant E and Kingon A 2001 Load characterization of high displacement piezoelectric actuators with various end conditions *Sensors Actuators* A **94** 19–24

Navapan-Traiphol N, Stutts A, Schwartz R W and Wood J 2004 Characterization and modeling of local electromechanical response in stress-based piezoelectric actuators *IEEE Int. Ultrasonics, Ferroelectrics and Frequency Control Joint 50th Anniversary Conf.* pp 56–9

Newnham R E and Ruschau G R 1991 Smart electroceramics *J. Am. Ceram. Soc.* **74** 463–80

Nothwang W D, Schwartz R W and Ballato J 2000 Simple plate resonator modeling and characterization of the effects of mass loading on the strain response of piezoelectric actuators *American Ceramic Society Annual Mtg (St. Louis, MO)*

Palmer J A, Dessent B, Mulling J F, Usher T, Grant E, Eischen J W, Kingon A I and Franzon P D 2004 The design and characterization of a novel piezoelectric transducer-based linear motor *IEEE/ASME Trans. Mechatron.* **9** 392–8

Saravanos D A 1997 Mixed laminate theory and finite element for smart piezoelectric shell structure *AIAA J.* **35** 327–1333

Schwartz R E and Narayanan M 2002 Development of high performance stress-biased actuators through the incorporation of mechanical pre-loads *Sensors Actuators* A **101** 322–31

Schwartz R W, Cross L E and Wang Q M 2001 Estimation of the effective piezoelectric d31 coefficients of Rainbow ceramics and comments on their enhanced performance *J. Am. Ceram. Soc.* **84** 2563–9

Smith R C 2005 *Smart Material Systems: Model Development* (PA, USA: Society for Industrial and Applied Mathematics)

Smith R C, Seelecke S, Ounaies Z and Smith J 2003 A free energy model for hysteresis in ferroelectric materials *J. Intell. Mater. Syst. Struct.* **14** 719–39

Soderkvist J 1996 Piezoelectric simulations validated on beams *ANSYS Conf. Proc.* pp 250–5

Takahashi S 1986 Longitudinal mode multilayer piezoelectric actuators *Am. Ceram. Soc. Bull.* **63** 1156–67

Taleghani B K and Campbell J F 1999 Non-linear finite element modeling of THUNDER piezoelectric actuators NASA smart structures and materials *Proc. SPIE Smart Struct. Integrated Syst.* **3668** 555–66

Thomson S P and Loughlan J 1995 The active buckling control of some composite column strips using piezoceramic actuators *Compos. Struct.* **32** 59–67

Uchino K 2000 *Ferroelectric Devices* (New York: Dekker) pp 57–66

Usher T and Sim A 2005 Nonlinear dynamics of piezoelectric high displacement actuators in cantilever mode *J. Appl. Phys.* **98** 064102–7

Wang Q M and Cross L E 1999 Tip deflection and blocking force of soft PZT-based cantilever RAINBOW actuators *J. Am. Ceram. Soc.* **82** 103–10

Wang Y D, Lin P R, Wang X L and McGreevy R L 2002 Grain-orientation-dependent residual stress and the effect of annealing in cold-rolled stainless steel *Acta Mater.* **50** 1717–34

Wieman R, Smith R C, Kackley T, Ounaies Z and Bernd J 2001 Displacement models for THUNDER actuators having general loads and boundary conditions *Proc. Int. Soc. Opt. Eng.* **4326** 253–63

Yoon H S, Washington G and Danak A 2005 Modeling, optimization, and design of efficient initially curved piezoceramic Unimorphs for energy harvesting applications *J. Intell. Mater. Syst. Struct.* **16** 877–88

Young D 1950 Vibration of rectangular plates by the Ritz method *J. Appl. Mech.* **17** 448–53

Zhang X D and Sun C T 1999 Analysis of a sandwich plate containing a piezoelectric core *Smart Mater. Struct.* **8** 31–40